Quantifying dimensional accuracy of a Mask Projection Micro Stereolithography System

Ameya Limaye and Dr. David Rosen
George W. Woodruff School of Mechanical Engineering
Georgia Institute of Technology
Atlanta GA 30332
Contact: Telephone number: 404 894 9668 Email: david.rosen@me.gatech.edu
Reviewed, accepted September 1, 2004

Abstract

Mask Projection Microstereolithography is capable for fabricating true three-dimensional microparts and hence, holds promise as a potential micro-fabrication process for micro-machine components. In this paper, the Mask Projection Micro-Stereolithography (MPμSLA) system developed at the Rapid Prototyping and Manufacturing Institute at Georgia Institute of Technology is presented. The dimensional accuracy of the system is improved by reducing its process planning errors. To this effect, the MPμSLA process is mathematically modeled. In this paper, the irradiance received by the resin surface is modeled as a function of the imaging system parameters and the pattern displayed on the dynamic mask. The resin used in the system is characterized to experimentally determine its working curve. This work enables us to compute the dimensions of a single layer cured using our system. The analytical model is validated by curing test layers on the system. The model computes layer dimensions within 5% error.

Introduction

Micro-sized machines have immense potential applications in a variety of fields like medical, industrial, entertainment etc. A number of these applications have been described in (Fujimasa, 1996). In order to realize such micromachines one of the challenges facing us is the development of a micro-fabrication technology. The micro fabrication process used to fabricate components for micromachines must be able to fabricate true three-dimensional geometries with a very high resolution and with a high degree of dimensional accuracy. The current micro-fabrication technologies like silicon etching and LIGA are capable of fabricating 2.5D micro-parts only. Mask Projection Micro Stereolithography (MPμSLA) is an adaptation of the Stereolithography process and is used to fabricate true three-dimensional geometries with a lateral resolution of up to 2 μm (Monneret et al., 1999). MPμSLA systems have been developed and studied by researchers for about a decade (Bertsch at al., 1997, Chatwin et al., 1998, Beluze et al., 1999, Chatwin et al., 1999, Farsari et al., 1999, Monneret at al., 1999, Bertsch et al., 2000, Farsari et al., 2000, Bertsch et al., 2001, Monneret at al., 2001, Hadipoespito et al., 2003). Most of the research published in these papers is concentrated on determining the resolution of the process and is experimental in nature. The issue of dimensional accuracy of the process has not been addressed. At the Rapid Prototyping and Manufacturing Institute (RPMI) at Georgia Institute of Technology, we have developed an MPμSLA system and modeled its part-building process in order to improve its dimensional accuracy.

Principle of Mask Projection Micro Stereolithography

The principle of operation of an MPμSLA system is illustrated in (Bertsch et al., 2000). The CAD model of an object to be built is sliced at different heights by a computer and the slices are stored as bitmaps. These bitmaps are displayed on the dynamic pattern generator, also called as the dynamic mask. Radiation from a light source is patterned by the bitmap displayed on the

dynamic pattern generator. The patterned radiation is focused onto the resin surface to cure a layer. The cured layer is coated with a fresh layer of resin and the next layer, of the required shape is cured over it. The micro-part is built by stacking layers one over the other.

MPµSLA system developed at RPMI

The schematic of the MPµSLA system developed at RPMI is illustrated in Figure 1.

The design of the system can be divided into three modules:

- Beam conditioning module: This module consists of a broadband light source, a pinhole, a collimating lens, and a filter. The pinhole is placed immediately after the light source to simulate a point source of light. The collimating lens collects the diverging light emerging from the pinhole and collimates it, i.e. sends out near about parallel rays of light. The filter allows only the radiation at 365nm to pass through, blocking out all other radiation.
- Imaging module: The imaging module consists of the Digital Micromirror Device, (DMD^{TM}), an imaging lens and a platform on which the micro part is built. The DMD^{TM} is an array of individually addressable, bi stable micro mirrors, which can be selectively oriented, to display any bitmap (Dudley et al., 2003). The bitmap displayed on the DMD serves as the object for the imaging system. The bitmap is imaged onto the platform by the imaging lens.
- Build module: This module consists of the platform, the translation stage and the resin vat. When a layer is cured on the platform, the platform is dipped inside the resin vat to coat the cured layer with a fresh film of resin. The thickness of the film coated on the already cured layer is controlled by accurately positioning the platform under the resin surface.

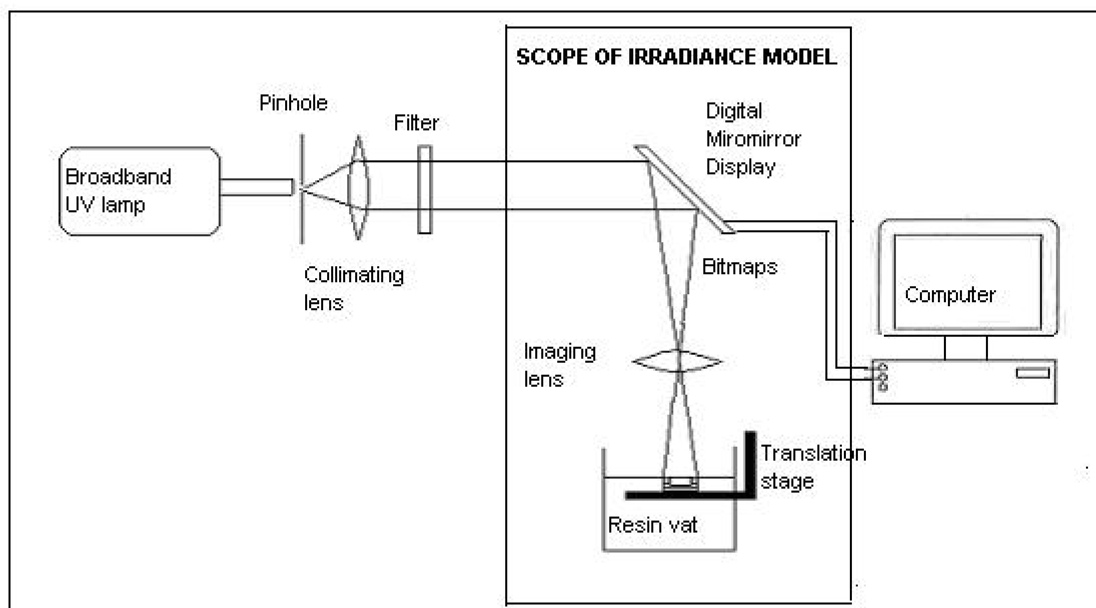

Figure 1 Schematic of the MPµSLA system developed at RPMI and the scope of the Irradiance model

Improving the dimensional accuracy of the process

The focus of this work is on improving the dimensional accuracy of the MPμSLA process by reducing the process planning errors. Process planning errors are those errors that can be created or reduced by changing the build process variables. There are three build process variables in the MPμSLA process:

- Pattern displayed on the DMD
- Time for which the bitmap is imaged onto the resin surface
- Layer thickness used while building the part

The effects of these variables on the cured layer's lateral dimensions are quantified by modeling the layer curing process as the Layer cure model.

A layer gets cured in two steps:

1. Patterned irradiation of the resin surface
2. Curing of the irradiated area of the resin down to the previously cured layer

In this paper, the first step is modeled by formulating the Irradiance model, which models the irradiance received by the resin surface as a function of the pattern displayed on the DMD and the imaging system parameters. The second step is modeled by characterizing the resin to experimentally determine the relation between the time of exposure and the depth to which the resin gets cured. The structure of the Layer cure model is shown in Figure 2.

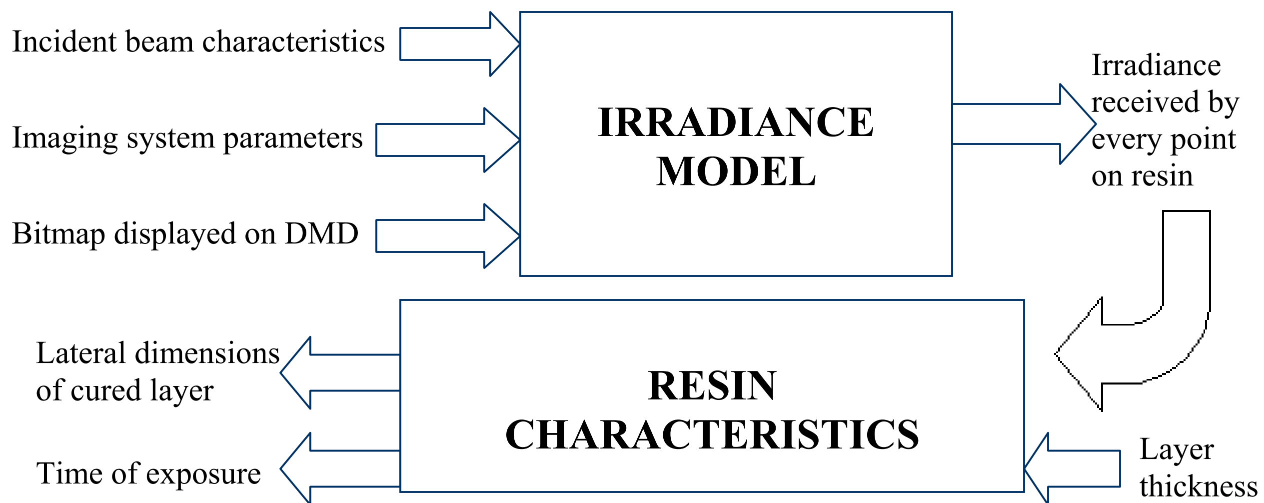

Figure 2 Structure of the Layer cure model

Irradiance model

Refer to Figure 1 for the scope of the Irradiance model. The irradiance distribution across the beam incident on the DMD is directly measured by mounting a radiometer in the path of the beam and traversing it along the beam's radius. This irradiance distribution is one of the inputs to the Irradiance model. The process of image formation is analytically modeled.

When a pattern displayed on the DMD is imaged onto the resin surface, all rays emanating from all points on the pattern are directed onto the resin surface by the imaging lens. Every ray irradiates the infinitesimal area centered at the point where it intersects the resin surface. The pattern can be assumed to be composed of n number of points: $p_1, p_{2,\ldots}p_n$, where $n \rightarrow \infty$. Since a UV lamp is used as the light source, the light beam incident on the DMD is not

completely collimated. So, rays are emitted in multiple directions from every point on the pattern. A cone of rays is emitted from each pattern point. There is an uncertainty as regards the angle of this cone and the distribution of energy within it. Since the beam incident on the DMD is fairly collimated, most of the energy is expected to be directed vertically downwards, parallel to the optical axis and so, the cone angle is expected to tend to zero. In general, the directions in which the rays are emitted can be represented by direction vectors $v_1, v_2, \ldots v_m$, where m→ ∞. The resin surface can be assumed to be composed of x number of points $pr_1, pr_2, \ldots, pr_x$, where x→ ∞. Refer to Figure 3.

We introduce a function δ, which evaluates whether a particular ray will strike an infinitesimal area centered on a given point on the resin surface or not. For example, $\delta(p_j, v_k, pr_i)$ will determine whether the ray originating from the point p_j on the bitmap in the direction of vector v_k will strike an infinitesimal area centered on point pr_i on the resin. If the ray does strike the infinitesimal area surrounding point pr_i, then $\delta(p_j, v_k, pr_i) = 1$. Else, $\delta(p_j, v_k, pr_i) = 0$.

The function δ is evaluated by adopting the exact ray tracing procedure as explained in (Smith, 1996). In an exact ray trace the path of every ray is traced through the lens, and the coordinates where it intersects the image plane are determined. The imaging system parameters are used in the evaluation of the function δ.

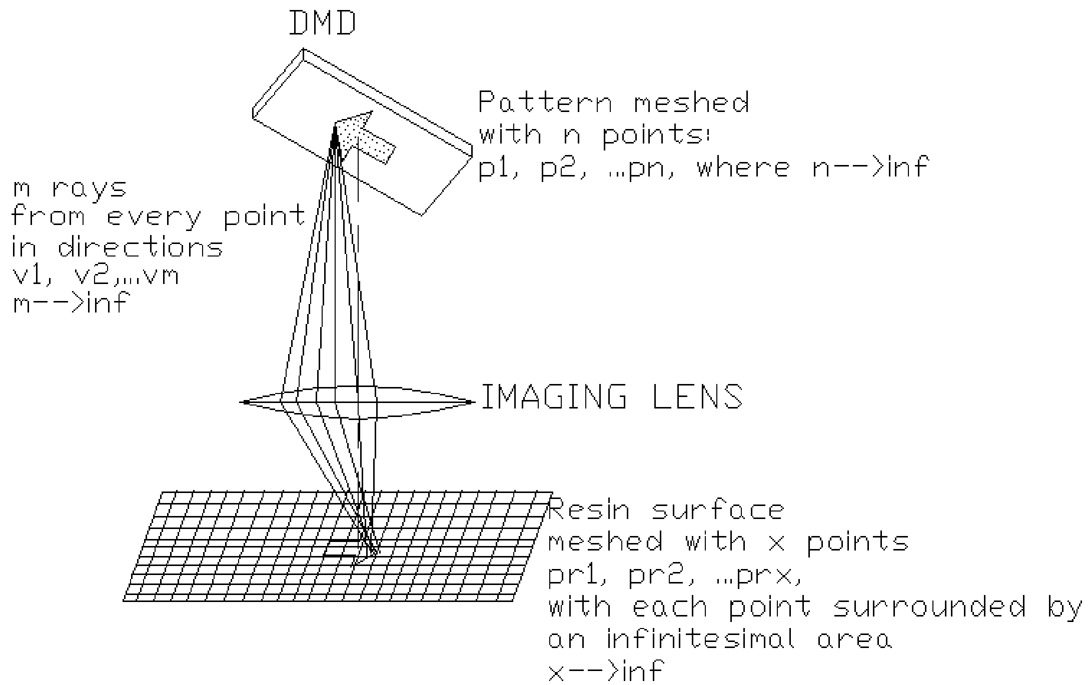

Figure 3 Nomenclature used in the theoretical derivations

The number of rays striking a point pr_i on the resin will be given by the function:

$$N(pr_i) = \sum_{j=1}^{n} \sum_{k=1}^{m} \delta(p_j, v_k, pr_i) \qquad (1)$$

Since the irradiance at a point on the resin surface is proportional to the number of rays striking that point, the irradiance can be given by:

$$H(pri) = c \sum_{j=1}^{n}\sum_{k=1}^{m} \delta(p_j, v_k, pr_i) \tag{2}$$

where c is a constant.

The constant c is calculated as follows:

Using a radiometer, the average irradiance across an aerial image can be measured. Let the average irradiance be H_{av}. The average number of rays striking a point on the resin surface will be given by (total number of rays/total number of points on the resin surface) = nm/x. So, nm/x rays correspond to an irradiance of H_{av}. The constant c is thus determined to be $H_{av}/(nm/x)$. Substituting for c in the equation (2),

$$H(pr_i) = (H_{av}x / nm)\sum_{j=1}^{n}\sum_{k=1}^{m} \delta(p_j, v_k, pr_i) \tag{3}$$

Equation (3) will give accurate results when $n \rightarrow \infty$, $m \rightarrow \infty$, and $x \rightarrow \infty$.

An assumption made while formulating equation (3) is that all rays carry the same amount of energy. This is not true because the irradiance across the beam incident on the pattern is not constant. So, the energy emitted by different points on the pattern is different. This effect can be accounted for by assigning weights to the rays emitted from different points on the pattern. If the weight assigned to the rays emitted from the jth point on the pattern (point p_j) is w_j, equation (3) can be modified as:

$$H(pr_i) = (H_{av}x / \sum_{j=1}^{n} w_j m)\sum_{j=1}^{n}\sum_{k=1}^{m} w_j \delta(p_j, v_k, pr_i) \tag{4}$$

The weights assigned to different pattern points are a function of the distance of that point from the center of the beam measured in the plane perpendicular to the direction of beam propagation. If w_j is the weight assigned to a pattern point, which is at a distance p from the center of the incident beam, then, w_j is given by:

$$w_j = f(p)$$

where $f(p)$ is the irradiance distribution across the beam. The irradiance distribution across the beam and hence, the weight function has been experimentally determined as:

$$w_j = 1 - 0.00086p - 0.00883p^2 \tag{5}$$

Time of exposure

If the resin is exposed for a time t, the point (pr_i) will receive exposure $E(pr_i)$ given by

$$E(pr_i) = H(pr_i)*t$$

If this exposure is greater than the threshold exposure required to initiate the photo polymerization reactions in the resin, also called as Critical Exposure (E_c), the resin will cure at that point.

$$\text{If } E(pr_i) \geq E_c\text{, resin will cure at point } pr_i \tag{6}$$

The variation in exposure with depth in the resin follows the Beer Lambert's law of absorption. So, the exposure at a depth z in the resin is given as:

$$E(pr_i,z) = E(pr_i)e^{-z/Dp}$$

where D_p is the depth of penetration of the resin. Again, if $E(pr_i,z) \geq Ec$, the resin will cure at that point. So, the depth to which the resin will cure at a point pr_i receiving irradiance $H(pr_i)$, (given by equation (4)), when exposed to irradiation for a time t is given by:

$$C_d(pr_i) = D_p \ln (H(pr_i)\, t)/E_c)$$

In order for the layers to bind to each other, the resin has to cure down to a depth at least equal to the layer thickness used while building the part.

If $C_d(x,y) \geq$ *layer thickness (LT),* the layers will bind. So, the condition for the layers to bind to each other is:

$$D_p \ln (H(pr_i)t/E_c) > LT$$

The minimum time of exposure is:

$$t_{min} = (E_c/minH(pr_i))\, e^{(LT/Dp)} \quad (7)$$

where $minH(pr_i)$ is the irradiance received by the point on the resin receiving the least irradiation.

Equation (7) gives the minimum time for which the resin must be exposed to radiation.

Characterizing the resin

The resin used with the MPμSLA system under consideration is the DSM SOMOS 10120 water clear resin. The values of E_c and D_p have been specified by the resin manufacturer to be 9.7 mJ/cm^2 and 0.16 mm respectively. Research on MPμSLA systems has shown that the experimentally observed values of E_c and D_p differ from their values specified by the manufacturer (Bertsch et al., 2000, Farsari et al., 2000, Hadipoespito, 2003). So, the resin needs to be characterized to experimentally determine the values of E_c and D_p.

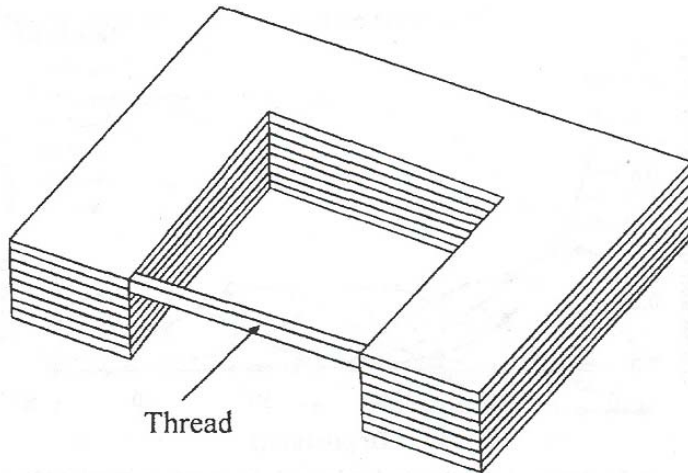

Figure 4 Polymer thread for cure-depth measurements

The following experiments are performed to determine the values of E_c and D_p: A polymer thread is cured, supported on a U-shaped micro-part as shown in Figure 4. The supporting micro-part is U shaped because it offers rigidity and is easy to handle and place under a microscope. The thread is located approximately at the center of the imaged area of the mask. The thread is cured by exposing it to radiation for different durations of time. By varying the time of exposure the radiant energy received by the thread is varied.

The thickness of the cured thread is plotted against the exposure received by the thread as shown in Figure 5. It can be seen from the plot that the cure depth is proportional to the natural logarithm of the exposure. From the plot, the value of E_c is found to be 9.6mJ/cm^2 and that of D_p as 0.056mm. Thus, the value of E_c agrees well with the manufacturer-specified value, while the value of D_p is much lower.

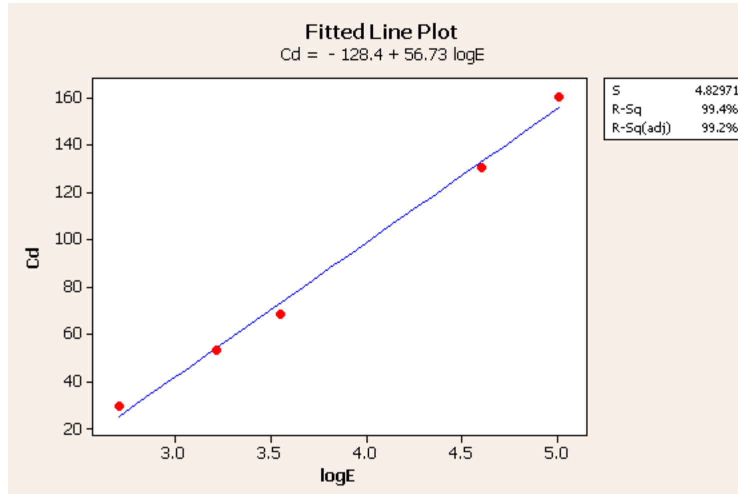

Figure 5 Working curve of resin

Summary of Layer cure model

The Layer cure model can compute the lateral dimensions of a cured layer and its minimum time of exposure using the following set of equations:

$$H(pr_i) = (H_{av}x / \sum_{j=1}^{n} w_j m) \sum_{j=1}^{n} \sum_{k=1}^{m} w_j \delta(p_j, v_k, pr_i)$$

(where x, n, and m → ∞ and $w_j = 1 - 0.00086p - 0.00883p^2$, p being the distance of the point pr_i from the center of the beam)

$E(pr_i) = H(pr_i)*t$

If $E(pr_i)) \geq E_c$, *resin will cure at point* pr_i

$t_{min} = (E_c/min\ H(pr_i))\ e^{(LT/Dp)}$

Numerical solution to the Layer cure model

To solve the Layer cure model, it is not possible to assign *n, m* and *x* values equal to ∞. In other words, we can mesh the pattern with only a finite number of points, trace rays only in a finite number of directions from every mesh point on the pattern and can evaluate the irradiance at only a finite number of points on the resin surface. So, while solving the model, we take larger and larger values of n, m for a chosen value of x till the irradiance distribution on the resin surface converges to its final value (Limaye, 2004).

Case Study: An application of the Layer cure model

Problem statement: A bitmap of dimensions as shown in Figure 6 is imaged on the surface of the DSM SOMOS 10120 resin to cure a layer 30 µm thick. Determine the lateral dimensions of the layer that will be cured and also compute the recommended time of exposure.

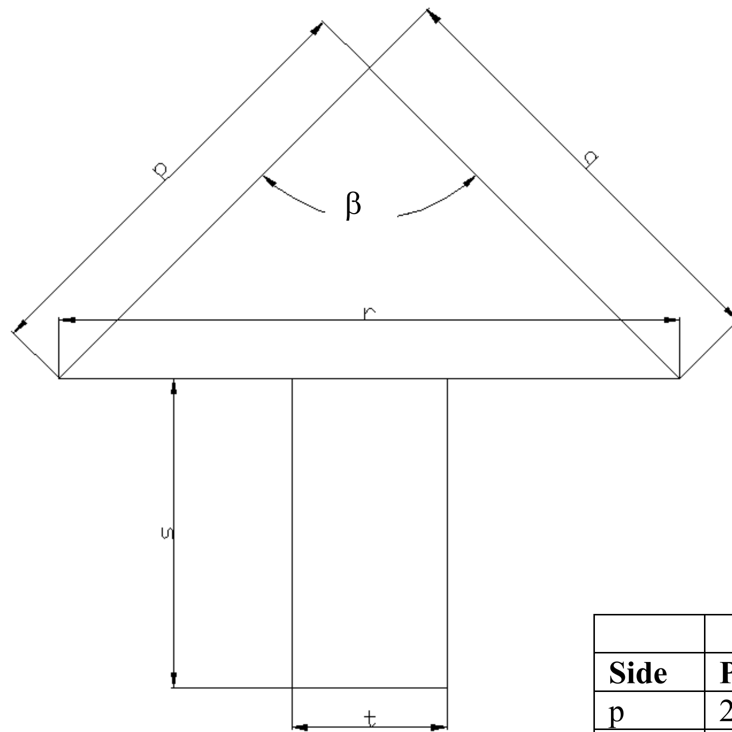

Side	Dimension Pixels	µm
p	283	3877
q	283	3877
r	400	5480
s	200	2740
t	50	685
β	90°	90°

Figure 6 Bitmap to be displayed on the DMD

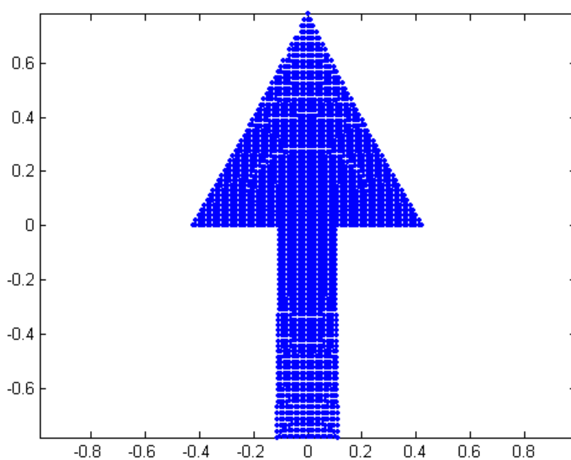

Figure 7 Aerial image of the arrow formed on the resin surface

Solution:

From the pitch of the micro mirrors on the DMD (known to be 13.7 µm) and the dimensions of the bitmap in pixels, the extents of the pattern are shown in Figure 6. This pattern is meshed with equally spaced points. As said earlier there is an uncertainty regarding the directions in which rays leave every point on the pattern. As a first approximation, we assume that the beam incident on the DMD is perfectly collimated and a single ray emanates from each point on the pattern, directed parallel to the imaging system optical axis, i.e. in the direction given by the direction cosines (0, 0, -1). Thus, a cone of rays of angle 0° is assumed to be emitted from each of the pattern points.

By tracing rays from all pattern points though the imaging lens, the irradiance received by the resin surface is computed. The numerical solution to the Irradiance model converges for the value of n = 9877, when the resin surface of 2mm x 1mm is meshed with 160 points (x = 160). The aerial image is shown in Figure 7. The average irradiance across the 2mm x 1mm area on the resin is measured to be 5mW/cm^2 ($H_{av}=5mW/cm^2$). From the Irradiance model, it is observed that the maximum irradiance is received at the center of the image and is equal to 10.17mW/cm^2. The minimum irradiance is received at the edges of the arrow and is 0.386 mW/cm^2. Hence, $minH(pr_i) = 0.386\ mW/cm^2$.

The minimum time for which the layer should be exposed to radiation is given as:

$t_{min} = (E_c/min\ H(pr_i))\ e^{(LT/Dp)}$

Using the experimentally determined values of E_c and D_p, the minimum time of exposure is calculated to be:

$t_{min} = 42.5s$

Testing the solution

The solution is tested by actually curing 15 test layers in resin by exposing them for 42.5s and comparing their dimensions with the dimensions returned by the Irradiance model. The picture of one of the sample layers is shown in Figure 8. The dimensions of the lengths p, q, r, s, t and angle β of the layer as shown in Figure 6 are compared. The dimensions of the 15 layers have been tabulated in Table 1.

Table 1 Comparison of calculated and experimental dimensions of layers

	Dimensions in microns					Angle in degrees
Layer #	p	q	r	s	t	β
1	900	875	887.5	775	212.5	53
2	887.5	850	887.5	762.5	200	60
3	912.5	900	887.5	775	212.5	55
4	912.5	887.5	875	775	212.5	53
5	912.5	900	887.5	787.5	225	57
6	900	875	875	787.5	212.5	53
7	937.5	912.5	887.5	787.5	212.5	56
8	900	900	875	787.5	212.5	57
9	912.5	900	887.5	775	212.5	57
10	925	900	887.5	787.5	212.5	55
11	900	875	875	775	212.5	51
12	912.5	900	887.5	787.5	212.5	52
13	912.5	887.5	887.5	787.5	212.5	54
14	887.5	875	875	775	212.5	56
15	912.5	900	887.5	787.5	212.5	54
Average	**908.3333**	**889.1667**	**883.3333**	**780.8333**	**212.5**	**54.86667**
Standard Deviation	**13.0817**	**16.27516**	**6.099375**	**7.999256**	**4.724556**	**2.356349**
3 σ	**39.24511**	**48.82549**	**18.29813**	**23.99777**	**14.17367**	**7.069047**
Percent Precision	**4.320562**	**5.491152**	**2.071486**	**3.073353**	**6.669961**	**12.88405**
Analytical dimensions	**887.5**	**887.5**	**846.3**	**780.1**	**223.7**	**53**
Error	**20.83333**	**1.666667**	**37.03333**	**0.733333**	**-11.2**	**1.866667**
Percent Error	**2.347418**	**0.187793**	**4.375911**	**0.094005**	**5.00671**	**3.40218**

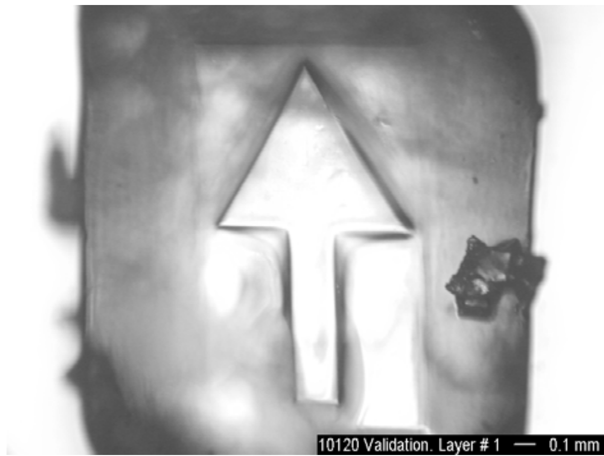

Figure 8 Arrow shaped layer

From Table 1, it can be seen that the model is accurate within 5% error. A point to notice is that though the angle at the tip of the arrow in the pattern is 90º, it is only about 55º in the cured layer. This is because of the angled mounting of the DMD and also because of the distortions caused by optical aberrations introduced by the imaging lens.

As stated earlier, the light beam incident on the DMD is not perfectly collimated. So, a cone of rays emits from each of the pattern points. In the case study above, we have assumed that the cone angle is zero. In order to test this assumption, the irradiance model was run by tracing rays contained in cones of angles varying from 0° to 1°. It was found that smaller cone angles agreed with the experimental dimensions better than larger cone angles. These results show that the cone angle of 0° can be assumed.

Some microparts cured on our system

A layer of required shape can be generated by displaying a distorted bitmap on the DMD. By running the Layer cure model iteratively, the bitmap required to cure a layer of the required shape is generated. Using this procedure, microparts of desired shape are obtained. The pictures some microparts cured using our system are shown in Figure 9.

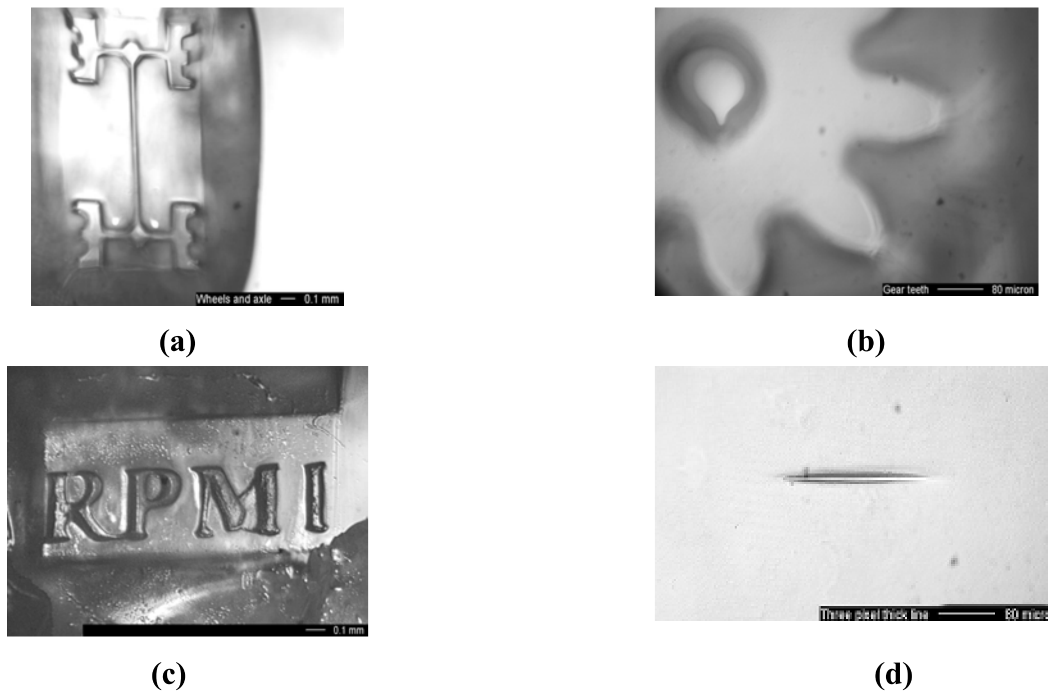

Figure 9 Pictures of some microparts cured on our system. (a) Four wheels and the axle of an SUV; (b) Teeth of a spur gear; (c) RPMI logo; (d) 6 µm thick line

Figure 9(a) is a picture of the four wheels and axle of an SUV. The axle is an overhang, cured on top of the four wheels. The part is made up of 9 layers, each 20 μm thick. In Figure 9(b), the picture of a spur gear is shown. The gear consists of 3 layers, each layer being 20 μm thick. The thickness of the teeth at the pitch circle diameter of the gear is 40 μm. The RPMI logo is shown in Figure 9(c). The logo consists of 2 layers, each of 30μm thickness. In Figure 9(d), the thinnest possible line cured using our system is shown. The width of the cured line is measured as 6μm. The width of the line computed by the Layer cure model is 6.2μm. This is the smallest feature that has been successfully cured using our system. So, the positive lateral resolution of our system is 6μm.

Conclusions and Future Work

Using the Layer cure model, the dimensions of any cured layer can be accurately calculated. This model can be used to determine the values of the variables that will accurately cure a layer of the required dimensions. From the agreement between the analytical and experimental results, we can conclude that ray tracing can be used to compute the image formation process of an MPμSLA build. The assumption that most of the rays from the pattern are emitted parallel to the imaging system optical axis is validated by the agreement between the experimental and analytical results.

It has been observed that the irradiance received at the central portion of the image (10.17mW/cm^2) is about 26 times that received at the edges (0.386 mW/cm^2). Due to this large variation in irradiance, the central portion of the image gets over-exposed and there is a loss of resolution at the central portion. A possible solution to this problem can be differential display of the pattern on the DMD, with the edges of the pattern displayed for a longer time than its central portion.

Using the irradiance model, the print-through and the overcure errors can be quantified and a compensation scheme for avoiding these errors can be formulated. This would allow us to cure micro-parts with accurate Z dimensions.

Acknowledgements

We gratefully acknowledge the support from the RPMI member companies and the Manufacturing Research Center at Georgia Tech.

References

Beluze L., Bertsch A., Renaud P., 1999, "Microstereolithography: a new process to build complex 3D objects", SPIE Symposium on design, test and microfabrication of MEMS/MOEMS, Vol. 3680, pp. 808-17.

Bertsch A., Zissi S., Jezequel J., Corbel S., Andre J., 1997, "Microstereolithography using liquid crystal display as dynamic mask-generator", Microsystems Technologies, pp.42-47.

Bertsch A., Lorenz H., Renaud P., 1999, "3D microfabrication by combining microstereolithography and thick resist UV lithography", Sensors and Actuators, Vol. 73, pp.14-23.

Bertsch A., Bernhard P., Vogt C., Renaud P., 2000, "Rapid prototyping of small size objects", Rapid Prototyping Journal, Vol. 6, Number 4, pp. 259-266.

Bertsch A., Bernhard P., Renaud P., 2001, "Microstereolithography: Concepts and applications", IEEE pp. 289-298.

Chatwin C., Farsari M., Huang S., Heywood M., Birch P., Young R., Richardson J., 1998, "UV microstereolithography system that uses spatial light modulator technology", Applied Optics, Vol. 37, pp.7514-22.
Chatwin C., Farsari M., Huang S., Heywood M., Young R., Bitch P., Claret-Tournier F., Richardson J., 1999, "Characterisation of epoxy resins for microstereolithographic rapid prototyping", International Journal of Advanced Manufacturing technologies, Vol. 15, pp.281-6.
Dudley D., Duncan W., Slaughter J., 2003, "Emerging Digital Micromirror Device (DMD) applications", SPIE proceedings, Vol. 4985.
Farsari M., Huang S., Birch P., Claret-Tournier F., Young R., Budgett D., Bradfield C., Chatwin C., 1999, "Microfabrication by use of spatial light modulator in the ultraviolet: experimental results", Optics Letters, Vol. 24, No. 8, pp. 549-50.
Farsari M., Claret-Tournier F., Huang S., Chatwin C., Budgett D., Birch P., Young R., Richardson J., 2000, "A novel high-accuracy microstereolithography method employing an adaptive electro-optic mask", Journal of Material Processing Technology 107, pp. 167-172.
Fujimasa I., 1996, "Micromachines: A new era in Mechanical Engineering", Oxford University Press.
Monneret S., Loubere V., Corbel S., 1999, "Microstereolithography using dynamic mask generator and a non-coherent visible light source", Proc. SPIE, Vol.3680, pp.553-561.
Monneret S., Provin C., Le Gall H., 2001, "Micro-scale rapid prototyping by stereolithography", 8th IEEE international conference on emerging technologies and factory automation (ETFA 2001), Vol. 2, pp. 299-304.
Hadipoespito G., Yang Y., Choi H., Ning G., Li X., 2003, "Digital Micromirror device based microstereolithography for micro structures of transparent photopolymer and nanocomposites", Proceedings of the Solid Freeform Fabrication Symposium, Austin Texas, pp. 13-24.
Limaye, A., 2004, "Design and Analysis of a Mask Projection Micro-Stereolithography System", Masters Thesis, Georgia Institute of Technology, Atlanta, GA.
Smith W., 1990, "Modern optical engineering: the design of optical systems", McGraw Hill.